GA–A25564

MONTE-CARLO SIMULATION OF HIGH HARMONIC FAST WAVE HEATING OF NEUTRAL BEAM IONS AND EFFECTS ON MHD STABILITY: VALIDATION WITH EXPERIMENTS

by

V. S. CHAN, A.D. TURNBULL, M. CHOI, M.S. CHU, and L.L. LAO

AUGUST 2006

GENERAL ATOMICS

DISCLAIMER

GA–A25564

MONTE-CARLO SIMULATION OF HIGH HARMONIC FAST WAVE HEATING OF NEUTRAL BEAM IONS AND EFFECTS ON MHD STABILITY: VALIDATION WITH EXPERIMENTS

by
V. S. CHAN, A.D. TURNBULL, M. CHOI, M.S. CHU, and L.L. LAO

This is a preprint of a paper to be presented at the Joint Varenna-Lausanne International Workshop on Theory of Fusion Plasmas, August 28 through September 1, 2006, in Varenna, Italy, and to be published in the *Proceedings.*

Work supported by
the U.S. Department of Energy under
DE-FG03-95ER54309

GENERAL ATOMICS PROJECT 03726
AUGUST 2006

Monte-Carlo Simulation of High Harmonic Fast Wave Heating of Neutral Beam Ions and Effects on MHD Stability: Validation With Experiments

V.S. Chan, A.D. Turnbull, M. Choi, M.S. Chu, and L.L. Lao

General Atomics, P.O. Box 85608, San Diego, California 92186-5608

Abstract. Experimentally, during fast wave (FW) radio frequency (rf) heating in DIII-D L-mode discharges, strong acceleration of neutral beam (NB) deuterium beam ions has been observed. Significant effects on the n/m = 1/1 sawtooth stability are also seen. Simulations using the Monte-Carlo Hamiltonian code ORBIT-RF, coupled to the TORIC full wave code, predict beam ion tails up to a few hundred keV, in agreement with the experiment. The simulations and experiment both clearly show a much greater efficiency for 4th harmonic FW heating than for 8th harmonic heating. Simple analyses of the kinetic contribution to the ideal magnetohydrodynamic (MHD) potential energy from energetic beam ions generated by FW heating yields reasonable consistency with the observations. A more detailed analysis shows a more complicated picture, however. Other physics effects such as geometry, plasma rotation, and the presence of a free boundary, play a significant role.

Keywords: Energetic ions, Fast wave heating, Sawtooth stabilization
PACS: Replace this text with PACS numbers; choose from this list:
http://www.aip.org/pacs/index.html

1. INTRODUCTION

In DIII-D experiments, strong acceleration of deuterium (D) neutral beam (NB) ions has been observed when fast waves (FW) were launched in a NB-heated plasma [1]. The FW also had a significant effect on the sawtooth (ST) characteristics of the discharge, which depended on the wave and the plasma conditions. In one discharge #96043 with 4th harmonic D heating from 60 MHz FW, giant sawteeth, among the largest observed in DIII-D were produced. For DIII-D discharge #122080, with 8th harmonic D heating by 116 MHz FWs, on the other hand, the observed ST were much smaller and more frequent. In addition, the experiments showed that the 4th harmonic heating was much more efficient in generating a high-energy tail [1]. These two discharges were well diagnosed and offer the possibility of comparing theoretical modeling of both the particle-wave interactions and the magnetohydrodynamic (MHD) behavior.

The control of ST and optimization of FW heating efficiency are critical issues for ITER. In addition, the theoretical understanding of both these aspects is fundamental to any basic plasma physics description and the experiments provide a unique opportunity to investigate MHD by treating the FW as a control tool, as well as to investigate wave-particle interaction physics using the MHD as a diagnostic tool.

The theory of MHD and of wave particle interactions has greatly matured in recent years. MHD has been shown to yield detailed quantitative and verified predictions of a wide variety of experiments in DIII-D [2,3]. The most glaring exception, however, is the detailed ST behavior [3]; non-ideal contributions to the stability of the m/n = 1/1 internal kink mode underlying sawteeth are well-known to be crucial. Among these non-ideal effects, kinetic contributions from a non-Maxwellian particle distribution are a key item [4,5]. Heating from FWs can produce such a high-energy tail in the distribution function. The theory for the resonant interaction between FWs and energetic ions is now well established even if computationally demanding.

The theory for both the ST stabilization and for the resonant wave particle interaction under hot plasma fusion conditions is at a stage where quantitative detailed comparisons can yield further understanding. Several studies have attempted to explain changes in ST behavior from analysis of the corrections to MHD stability of the internal kink due to an energetic ion population [4,6,7] using the Porcelli model [4]. Qualitative agreement with the observed ST characteristics is generally very good [6-9].

The agreement has provided confidence that the essential model is basically correct. Nevertheless, the comparisons so far have generally relied on several simplifications. Foremost is the reliance on analytic estimates for the MHD and other contributions to the normalized total perturbed energy $\delta\hat{W} = \delta\hat{W}_{\mathrm{MHD}} + \delta\hat{W}_{\mathrm{KO}} + \delta\hat{W}_{\mathrm{F}}$. Most estimates of $\delta\hat{W}_{\mathrm{MHD}}$ utilize the analytic result of Bussac et al. [10] though recent attempts [11] have been made at incorporating corrections for non-circular cross section and for finite aspect ratio [12]. Boundary conditions can also be important; allowing the boundary to be perturbed can increase growth rates considerably and, significantly, it also changes the marginal stability point [13-15]. In addition, the estimates for $\delta\hat{W}_{\mathrm{KO}}$ and $\delta\hat{W}_{\mathrm{fast}}$ are based on integration over the trapped and fast particle distribution functions convolved with the Bussac model for the eigenfunction. This model is generally a good approximation [13,14,16] but it can break down in some cases of practical interest.

The present work is intended to address these issues by using more realistic estimates of the key contributions within the context of the Porcelli model and comparing with the DIII-D experiments. The following section considers the simulations of the FW particle interactions. The ORBIT-RF code [17] is used in conjunction with the 2D full wave code TORIC [18] which provide the FW amplitudes. The simulations are consistent with observational signatures that will be discussed in Section 3. Section 4 briefly reviews the key assumptions that go into the Porcelli ST stabilization model. Comparisons with the observed ST behavior are given in the discussion in Section 5 and a summary of the implications from this study is provided in Section 6.

2. SIMULATION OF WAVE PARTICLE INTERACTIONS

Quasi-linear (QL) theory describes the resonant interaction between the FW and plasma ions as a diffusive process in velocity space, based on the assumption that the relative phase between the FW and ions tends to be decorrelated. In a collisionless,

high-temperature plasma, the relative phase is randomized on a time scale much faster than the thermal slowing down time. After each "kick" from the rf electric field as the ion passes through the resonance, the ions sample different local cyclotron frequencies ω_c and parallel wave number $k_{||}$ if the wave amplitude is large enough, leading to a strong decorrelation. The wave amplitudes for the experiments being considered satisfy the validity of this model.

QL diffusion in velocity space is modeled in the ORBIT-RF Monte-Carlo Hamiltonian code using a simplified rf-induced random walk. The change in magnetic moment μ from the wave, $\Delta\mu_{RF}$, is expressed as the sum of a time independent mean change $\overline{\Delta\mu_{RF}}$ and a rapidly fluctuating part $\tilde{\Delta\mu}_{RF}$ [17]. Then

$$\Delta\mu_{RF} = \overline{\Delta\mu_{RF}} + R_s \sqrt{\tilde{\Delta\mu}_{RF}^{\,2}} \equiv \int_{\Delta t} \frac{q^2 l^2 \Omega^2}{\omega^2 B^2} \frac{\partial D_{\perp l}}{\partial \mu} dt + R_s \int_{\Delta t} \frac{2q^2 l^2 \Omega^2}{\omega^2 B^2} D_{\perp l} dt \quad . \quad (1)$$

Δt is taken to be a wave-particle interaction time. The QL diffusion operator is given by

$$D_{\perp \ell}(k_{||}) = \frac{\pi B}{m_i} K\delta(\omega_l) \sum_{m'} \left[E_+^{m'} J_{l-1}\left(k_\perp^{m'} \rho_i\right) \right]^* \sum_m \left[E_+^m J_{l-1}\left(k_\perp^m \rho_i\right) \right] \quad . \quad (2)$$

Here, J_{l-1} is the $(l-1)$'th order Bessel functions of the first kind, $\rho_i = v_\perp/\Omega_i = \sqrt{2\mu B/\Omega_i}$ is the ion gyroradius, and E_+^m represents the mth poloidal Fourier mode of the wave electric field; $E_+ \equiv \sum E_+^m e^{im\theta}$. K is a factor ~1. The wave fields and wave numbers, E_+^m, $k_\perp^m$, and $k_{||}^m$ are calculated using unit current wave fields from the code TORIC [18], rescaled to match the experimental input power. A single toroidal mode number n is assumed. As an approximation only the dominant poloidal harmonic is used in thus ORBIT-RF calculation [17]. The ORBIT-RF code then follows the particle orbits by solving the Hamiltonian Guiding Center Drift equations in the background equilibrium fields [5] between successive rf kicks, ignoring the perturbed fields from the wave.

3. EXPERIMENTAL CONFIRMATION OF SIMULATION

The simulations were applied to the two L-mode DIII-D NB heated discharges #96043 and #122080. Figure 1 shows the resultant calculated distribution functions for the injected beam ions (E_I = 80 keV) in the two cases. In both, the distribution follows a slowing down form for $E < E_I$ with a strong tail extending up to 600 keV for discharge #96043 and to 200 keV for discharge #122080. The resonance radius is located near the magnetic axis in both cases.

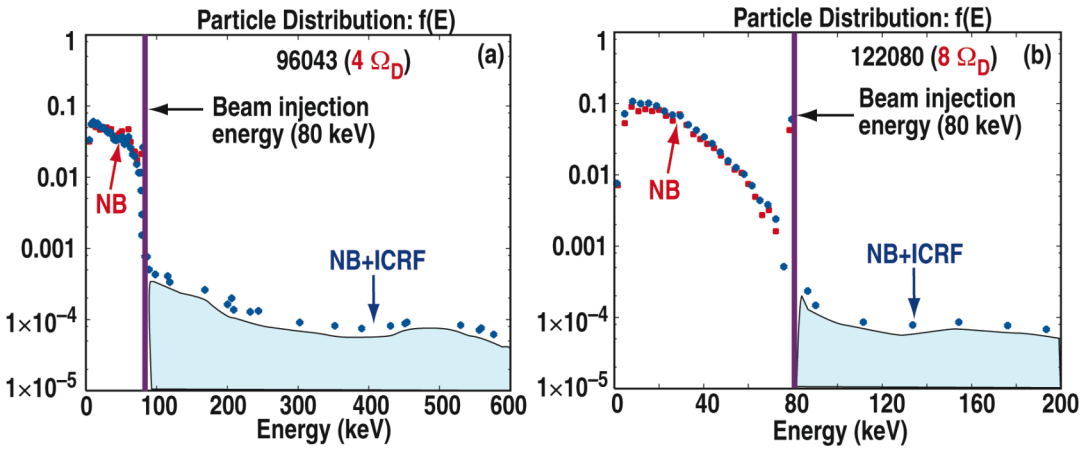

FIGURE 1. Calculated ion distribution function from ORBIT-RF simulations for discharges (a) #96043 at 2020 ms and (b) #122080 at 2700 ms.

The cross sections were similar but the plasma conditions were quite different. Figure 2 shows the reconstructed pressure and safety factor profiles. Note in particular the smaller radius for the $q=1$ surface in #122080. Table I shows the relevant parameters for the two discharges.

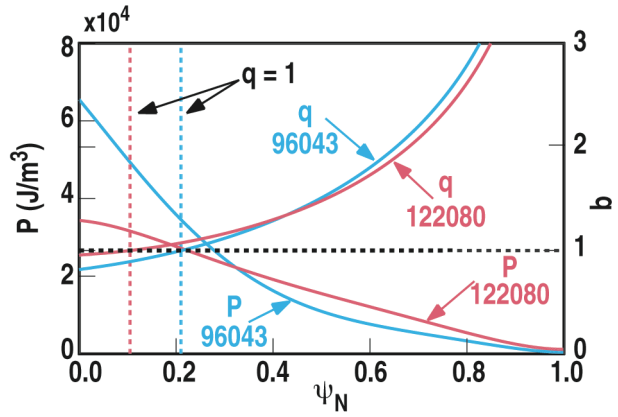

FIGURE 2. Reconstructed safety factor (right scale) and pressure profiles (left scale) for discharges #96043 and #122080. Indicated are the position of $q=1$ for each.

Generation of a high-energy tail in both cases was indicated experimentally by significant neutron enhancement during the time over which the rf was applied. The enhancement was considerably larger for discharge #96043 for which the ORBIT-RF simulations predicted a longer high-energy tail, despite the lower NB power and the lower input rf power.

Experimentally, the two discharges exhibited very different ST behavior during the time the FW was applied. This is seen in Figure 3, which shows the frequency spectrum of the MHD activity. In both, the sawteeth crashes are seen as the $n=1$ bursts. Before the FW, they are similar, with sawteeth occurring about every 100 ms. For discharge #122080, the ST behavior is unaffected by the FW. However, in discharge #96043 there is an immediate ST when the FW is turned on, followed by a

prolonged ST-free period and subsequently a large ST crash associated with considerable subsequent higher n activity. The simulations and equilibrium reconstructions were performed at the time of this ST crash at 2020 ms.

TABLE 1. Relevant Parameters for Discharges #96043 and 122080.

Shot No.	P_{NB} (MW)	P_{RF} (MW)	$n_e(0)$ (cm^{-3})	$T_e(0)$ (keV)	$T_i(0)$ (keV)	$B(0)$ (T)	ω_{*i} (rad/s)	ω_{*c} (rad/s)	τ_A (μs)
96043	2.7	1.0	4.7×10^{13}	3.4	2.9	1.9	9.7×10^{3}	-1.9×10^{4}	4.4
122080	5.0	1.7	6.8×10^{13}	1.5	1.9	1.8	9.3×10^{3}	-6.8×10^{4}	5.4

Shot No.	β_{pl}	β_{io}	β_{pc}	β_{ph} Before	β_{ph} After	ω_{Dh} Before (rad/s)	ω_{Dh} After (rad/s)
96043	0.204	9.14×10^{-3}	0.143	0.065	0.080	3.6×10^{4}	4.0×10^{4}
122080	0.043	9.17×10^{-3}	0.185	0.020	0.199	4.7×10^{3}	5.0×10^{3}

Shot No.	ψ_{pl}	S	l_{i1}	ε_1	κ_1	s_1	s_{crit}	$\hat{\rho}$
96043	0.202	1.23×10^{7}	0.584	0.145	1.27	0.437	4.93×10^{-2}	7.196×10^{-3}
122080	0.096	3.35×10^{6}	0.543	0.108	1.33	0.110	4.27×10^{-2}	1.185×10^{-2}

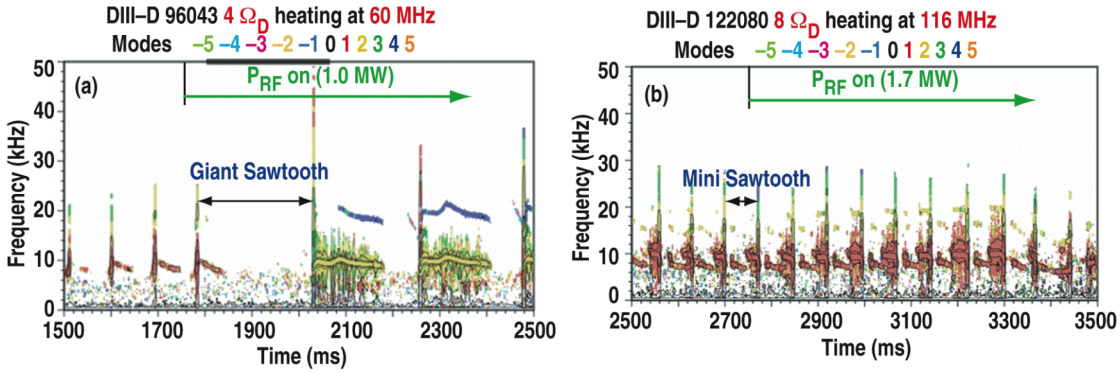

FIGURE 3. MHD spectral analysis for discharges (a) #96043 and (b) #122080. The time at which the FW was turned on is indicated. The mode identification is color coded as indicated.

In discharge #122080, the ST continued as small and frequent "mini-sawteeth", whereas discharge #96043, with the larger fast ion tail population expected from the simulations, exhibited "giant-sawteeth" from the time the FW was initiated. This is qualitatively consistent with the expectation that the fast ion population has stabilized the $m/n = 1/1$ mode in the latter case. According to the conventional interpretation, the ST finally occurs after the internal energy has built up considerably, producing a delayed, much larger "giant sawtooth". A more detailed comparison can be made by quantitatively applying the Porcelli model for the two discharges.

4. PORCELLI SAWTOOTH MODEL

The model developed in Ref. [4] to describe ST onset has been quite successful in explaining the ST characteristics of a variety of sawtoothing discharges [8,9,11,19-21]. It represents the standard model for predicting ST behavior in ITER [4,9,15,22]. The ideal MHD potential energy δW_{MHD} for the $m/n = 1/1$ internal kink mode, modified by kinetic contributions from thermal ions δW_{KO} and fast ions δW_{fast} plays a key role.

Sawtooth crashes are triggered when one of the following conditions is met [4]:

$$-\delta\hat{W}_{\mathrm{core}} = -\left(\delta\hat{W}_{\mathrm{MHD}} + \delta\hat{W}_{\mathrm{KO}}\right) > C_{\mathrm{h}}\omega_{\mathrm{Dh}}\tau_{\mathrm{A}} \tag{3}$$

$$-\delta\hat{W} = -\left(\delta\hat{W}_{\mathrm{MHD}} + \delta\hat{W}_{\mathrm{KO}} + \delta\hat{W}_{\mathrm{case}}\right) > 0.5\omega_{*\mathrm{i}}\tau_{\mathrm{A}} \tag{4}$$

$$-C_{\mathrm{p}}\hat{\rho} < -\delta\hat{W} < 0.5\omega_{*\mathrm{i}}\tau_{\mathrm{A}};\ \text{and}\ \omega_{*\mathrm{i}} < C_{*}\gamma_{\mathrm{p}}\quad . \tag{5}$$

Here, ω_{Dh} is the average toroidal procession drift frequency of the fast ions calculated from ORBIT-RF, τ_{A} is the Alfvén time, $\omega_{*\mathrm{i}}$ the thermal ion diamagnetic frequency, and the parameter $C_{\mathrm{h}} \sim 0.4$. Also, $\gamma_{\mathrm{p}} = C_{\mathrm{p}}\hat{\rho}S^{-1/7}s_1^{6/7}\tau_{\mathrm{A}}^{-1}$ where $C_{\mathrm{p}} = 1$, $C_{*} = 3$, $S = \tau_{\mathrm{m}}/\tau_{\mathrm{A}}$ is the Lundquist number, $\hat{\rho} = \rho_{\mathrm{i}}/r_1$ is the ion Larmor radius normalized to the radius of the $q = 1$ surface, and $s_1 \equiv r_1\ dq/dr\big|_{\mathrm{r=r_1}}$ is the shear at $q = 1$. The Alfvén time is $\tau_{\mathrm{A}} = \sqrt{3}\ R/V_{\mathrm{A}}$. $\tau_{\eta} = 4\pi r_1^2/\eta_{\|}c^2$ is the resistive diffusion time.

The ideal perturbed potential energy is normalized as

$$\delta\hat{W}_{\mathrm{MHD}} = 4\delta W \Big/ s_1|\xi_0|^2\varepsilon_1^2 R\left(B_0^2/\mu_0\right) \tag{6}$$

where $|\xi_0|$ is the displacement amplitude of the 1/1 mode inside $q = 1$. Then $\delta\hat{W}_{\mathrm{KO}}$ is a Kruskal-Oberman contribution from thermal trapped ions and $\delta\hat{W}_{\mathrm{fast}}$ is the kinetic fast ion contribution. The basic condition for instability of the ideal internal kink mode is $\delta\hat{W}_{\mathrm{MHD}} < 0$. The Kruskal Oberman term is invoked when the mode frequency exceeds the thermal ion diamagnetic frequency; $\omega > \omega_{*\mathrm{i}}$. This translates into a condition that $\delta\hat{W}_{\mathrm{KO}} > \omega_{*\mathrm{i}}\tau_{\mathrm{A}}$.

Traditionally, $\delta\hat{W}_{\mathrm{MHD}}$ has been obtained from an analytic model by Bussac, et al. in the limit of a large aspect ratio torus with circular cross section and a parabolic pressure profile inside $q = 1$ [10]. Several extensions to shaped cross sections have been suggested, most notably the extension by Porcelli using $\delta\hat{W}_{\mathrm{MHD}} = \delta\hat{W}_{\mathrm{B}} + \delta\hat{W}_{\kappa}$, or

$$\delta\hat{W}_{\mathrm{MHD}} = \frac{-9\pi\left(l_{\mathrm{i}1} - \frac{1}{2}\right)}{s_1}\,\varepsilon_1^2\left(\beta_{\mathrm{p}1}^2 - \beta_{\mathrm{pc}}^2\right) + \frac{-18\pi\left(l_{\mathrm{i}1} - \frac{1}{2}\right)^3}{s_1}\left(\kappa_1 - \frac{1}{2}\right)^2 \qquad (7)$$

$\beta_{\mathrm{p}1}$ is the poloidal β integrated inside $q = 1$ and β_{pc} is the critical ideal limit; in the Bussac model, $\beta_{\mathrm{pc}} \cong 0.3$. l_{i1} and κ_1 are the internal inductance and elongation at $q = 1$.

The Bussac model predicts that to lowest order in inverse aspect ratio, the unstable mode has the structure of a "top hat" in which $\xi(r) = \xi_0$ for $r < r_1 - (1/2)\varepsilon$ and $\xi(r) = 0$ for $r > r_1 + (1/2)\varepsilon$, with an inertial layer of width ε around $q = 1$. A smooth transition of $\xi(r)$ maintains $\nabla \cdot \xi = 0$ such that $\xi_{\mathrm{pol}} \sim r(\partial\xi_{\mathrm{r}}/\partial \mathrm{r})$ remains finite. This yields a finite kinetic energy and growth rate, given by $\gamma_{\mathrm{MHD}}^2 = \delta W/\delta K$ where $\delta K = (1/2)/\rho_{\mathrm{m}}(r)|\xi|^2 r dr$ (ρ_{m} is the mass density). In this limit, one finds $\gamma_{\mathrm{MHD}}\tau_{\mathrm{A}} \equiv \delta\hat{W}_{\mathrm{B}}$, identical to the result obtained for a cylindrical screw pinch [23]. The higher order modification to the mode from the small but crucial $m = 2$ harmonic which connects the internal region $r < r_1$ to $r > r_1$ is ignored in obtaining the linear dependence of γ_{MHD} on $\delta\hat{W}_{\mathrm{B}}$ but is an important part of $\delta\hat{W}_{\mathrm{B}}$ itself. With regard to the shaping corrections, in the cases of interest here, $\kappa \sim 2$ and these must be included.

The Kruskal Oberman term is also obtained analytically from integrating the trapped particle distribution over the zeroth order model displacement in the limit $\varepsilon \to 0$. Thus, this is strictly valid only in the large aspect ratio circular cross section limit. The result is $\delta\hat{W}_{\mathrm{KO}} = 0.6 C_{\mathrm{p}}\varepsilon_1^{1/2}\beta_{\mathrm{io}}/s_1$ with $C_{\mathrm{p}} \equiv (5/2)\int_0^1 x^{3/2}\, p_{\mathrm{i}}(x)/p_{\mathrm{io}}\, dx$ and $x = r/r_1$.

The fast particle contribution $\delta\hat{W}_{\mathrm{fast}}$ is obtained from integrating the fast particle distribution function convolved with the zeroth order internal kink displacement. The result from Ref. [4] is

$$\delta\hat{W}_{\mathrm{fast}} = C_{\mathrm{f}}\varepsilon_1^{3/2}\beta_{\mathrm{pf}}^*/s_1 \qquad (8)$$

with $C_{\mathrm{f}} = C_{\mathrm{p}}(\omega/\omega_{\mathrm{Di}}) \sim 1$. β_{pf}^* is the fast trapped ion contribution to the poloidal β_{p}.

The factors in the normalizations for $\delta\hat{W}_{\mathrm{MHD}}$, $\delta\hat{W}_{\mathrm{KO}}$, and $\delta\hat{W}_{\mathrm{fast}}$ also need to be estimated. The radius of the $q = 1$ surface r_1 must be replaced by an equivalent radius and used in evaluating both $\varepsilon_1 = r_1/R_0$ and $s_1 \equiv r_1\ dq/dr|_{\mathrm{r}=\mathrm{r}_1}$. Porcelli proposes using $r_1^* = \kappa_1^{1/2} r_1$ where r_1 is the midplane minor radius. A more general expression is $r_1^* = V^{1/2}/(2\pi^2 R_0)$. $|\xi_0|^2$ is also assumed to be the constant displacement inside $q = 1$. In reality, $\xi(r)$ will have some radial dependence. If the dependence is weak, an average inside $q = 1$ or a maximum can be used. When the dependence is much stronger, the model becomes questionable. The quantities $\omega_{*\mathrm{i}}$, ω_{Dh}, S, etc., may be

estimated from the experimental discharge equilibrium from averages at the $q = 1$ surface, and are given in Table 1. However, it needs to be kept in mind that the equations and conditions where they appear are essentially derived from local models.

5. δW ANALYSIS OF ST STABILITY

In the absence of a direct measurement of the fast ion distribution function, the expected fast ion stabilization of the ST can be used as an indirect diagnostic. The ultimate aim is to compare the observed ST phenomena directly with the predictions. This is a more ambitious proposal than the comparisons of the ST cycle [4,6,7-9, 11,15,19,22] made in earlier work, where the individual terms involved in the trigger criteria vary rapidly during the cycle [4]. In searching for the time at which they cancel, systematic errors in individual terms are quickly swamped by the rapidly changing terms so that the cancellation occurs only a short time either before or after the correct time. Thus, the analysis of the ST onset time is well posed, since it is relatively forgiving of approximations used in evaluating the terms. The approximations can be in either the actual models for the individual terms (such as the Bussac expression for δW_{MHD}) or the equilibria reconstructed and used as input to the models. These studies therefore provide good evidence that the basic trigger mechanisms in the Porcelli model are correct, even if evaluated with approximate expressions.

The analysis here proposes to evaluate each of the terms at a specific time in the ST cycle to compare predictions between two discharges in order to extract information about the fast particle distribution functions. This requires an accurate evaluation of all the terms. The quality of equilibrium reconstructions in DIII-D [2] coupled with numerical tools for evaluating the key terms in the trigger mechanism – notably $\delta\hat{W}_{\mathrm{MHD}}$, $\delta\hat{W}_{\mathrm{KO}}$, and $\delta\hat{W}_{\mathrm{fast}}$ – places this more ambitious goal within reach. Since the interest is in the fast particle term, the key contribution made is an evaluation of this term using the fast particle distribution evaluated from the ORBIT-RF and TORIC simulations.

When the FW is turned on in discharge #96043, the ST amplitude and period become larger and longer, whereas the ST in discharge #122080 are unaffected. From Section 3, the calculated fast ion tail from the FW is considerably larger and extends to higher energies in discharge #96043. A tentative hypothesis would therefore be that the 1/1 mode is stabilized in that case by an increase in $\delta\hat{W}_{\mathrm{fast}}$ from β_{ph}.

The ST predictions for the two discharges are evaluated using two different estimates for $\delta\hat{W}_{\mathrm{MHD}}$, which is the most important term competing with $\delta\hat{W}_{\mathrm{fast}}$. The fast ion contribution is evaluated using $\delta\hat{W}_{\mathrm{fast}}$ from Eq. (8) with

$$\beta_{\mathrm{ph}} = \frac{-2\mu_0}{B_{\mathrm{p}}^2} \int_0^1 x^{3/2} \frac{dp_{\mathrm{h}}}{\mathrm{d}x}\, dx \qquad (9)$$

using the trapped fast particle pressure $p_h(x)$ evaluated from the ORBIT-RF and TORIC codes. The term $\delta\hat{W}_{KO}$ is evaluated using the equilibria reconstructed from the discharge data. Each of the trigger options is evaluated.

Table 2 shows the results of the analysis using the Bussac model, including the corrections due to shaping, just before a ST event for the two discharges. $\sqrt{V(q=1)}/2\pi^2 R_0$ is used for r_1.

TABLE 2. Porcelli Criterion Analysis for Discharges #96043 at 2020 ms and #122080 at 2700 ms

	#96043	#122080
$\delta\hat{W}_{KO} > \omega_{*i}\tau_A$	No	Yes
$\delta\hat{W}_{KO}$	Theory not applicable	$+1.5\text{x}\,10^{-2}$
$\delta\hat{W}_{fast}$	$+1.0\text{x}\,10^{-2}$	$+6.6\text{x}\,10^{-3}$
$\delta\hat{W}_B$	$-2.4\text{x}\,10^{-3}$	$+4.2\text{x}\,10^{-3}$
$\delta\hat{W}_\kappa$	$-1.4\text{x}\,10^{-3}$	$-1.1\text{x}\,10^{-3}$
$\delta\hat{W}_{MHD} = \delta\hat{W}_{Bussac} + \delta\hat{W}_\kappa$	$-3.8\text{x}\,10^{-3}$ (ideal unstable)	$+2.9\text{x}\,10^{-3}$ (ideal stable)
$\delta\hat{W} = \delta\hat{W}_{MHD} + \delta\hat{W}_{fast} + \delta\hat{W}_{KO}$	$+6.2\text{x}\,10^{-3}$ (stable)	$+2.5\text{x}\,10^{-2}$ (stable)
$-\delta\hat{W}_{core} > c_h\omega_{Dh}\tau_A$	No	No
$-\delta\hat{W} > 0.5\omega_{*i}\tau_A$	No	No
$-c_p\hat{\rho} < -\delta\hat{W} < 0.5\omega_{*i}\tau_A,\ s_1 > s_{crit}$	Yes (trigger on)	No
β_{pl}^{crit}	+0.065	+0.035
$\delta\hat{W}_M$	$-7.8\text{x}\,10^{-3}$ (ideal unstable)	$-4.8\text{x}\,10^{-4}$ (ideal unstable)
$\delta\hat{W} = \delta\hat{W}_M + \delta\hat{W}_{fast} + \delta\hat{W}_{KO}$	$+2.2\text{x}\,10^{-3}$ (stable)	$+2.1\text{x}\,10^{-2}$ (stable)
$-\delta\hat{W}_{core} > c_h\omega_{Dh}\tau_A$	No	No
$-\delta\hat{W} > 0.5\omega_{*i}\tau_A$	No	No
$-c_p\hat{\rho} < -\delta\hat{W} < 0.5\omega_{*i}\tau_A,\ s_1 > s_{crit}$	Yes (trigger on)	No

This analysis would predict that in discharge #96043 the ST would be stabilized against the ideal mode by the fast ion contribution: $\delta\hat{W} = \delta\hat{W}_{MHD} + \delta\hat{W}_{fast} > 0$. At this time, $\delta\hat{W}_{KO} < \omega_{*i}\tau_A$ so $\delta\hat{W}_{KO}$ should be neglected. Nevertheless, the third criterion for a ST is satisfied; $0 < \delta\hat{W} < C_p\rho$. This corresponds to destabilization of the resistive internal kink in the so-called ion-kinetic regime [19], and is consistent with the interpretation that the fast ions stabilized the internal kink, delaying the ST onset until this criterion was triggered and a large ST resulted.

For discharge #122080, $\delta\hat{W}_{KO} > \omega_{*i}\tau_A$ but none of the trigger criteria are satisfied. In fact, the ideal $\delta\hat{W}_{MHD} = \delta\hat{W}_B + \delta W_\kappa > 0$ suggesting that the ideal mode is already stable. This would be inconsistent with the observed sawtoothing in this discharge. However, there are several explanations. First, the result $\delta\hat{W}_{MHD} > 0$ is also inconsistent with a numerical calculation of the ideal stability using the GATO code [24], since this predicts an internal kink instability. Martynov et al. [15] have shown that the estimate $\delta\hat{W}_\kappa$ suggested by Porcelli, et al. becomes inaccurate and does not match the numerically computed growth rates at $\kappa \gtrsim 1.4$, and that the scaling

$\delta\hat{W}_{\mathrm{MHD}} \sim \left(\beta_{\mathrm{p}}^2 - \beta_{\mathrm{pc}}^2\right)/s_1$ breaks down. In that study, $\delta\hat{W}_{\mathrm{MHD}} = \gamma\tau_{\mathrm{A}}$ calculated from the analytic formulae were compared with numerically computed $\gamma_{\mathrm{MHD}}\tau_{\mathrm{A}} \cong (\delta W/\delta K)^{1/2}$ values. A much better fit to the numerical results was found to be

$$\delta\hat{W}_{\mathrm{M}} \equiv \gamma_{\mathrm{MHD}}\tau_{\mathrm{A}} = 0.45\frac{\varepsilon_1\kappa_1}{1+7\varepsilon_1 s_1}\left(\beta_{\mathrm{p1}} - \beta_{\mathrm{pc}}^*\right) \tag{10}$$

with $\beta_{\mathrm{pc}}^* = 0.7 - 0.5\kappa_1$. Note in particular the linear dependence on $\left(\beta_{\mathrm{p1}} - \beta_{\mathrm{pc}}^*\right)$ and the replacement of the $1/s_1$ dependence by the much weaker $(1+7\varepsilon_1 s_1)^{-1}$ dependence with no pole at zero shear. Table 2 also shows the results of the ST trigger analysis using $\delta\hat{W}_{\mathrm{M}}$ as an estimate for $\delta\hat{W}_{\mathrm{MHD}}$. The result for discharge #96043 is qualitatively unchanged. For discharge #122080, however, $\delta\hat{W}_{\mathrm{MHD}}$ is now negative, consistent with the numerically calculated ideal instability. However, $\delta\hat{W}_{\mathrm{MHD}} + \delta\hat{W}_{\mathrm{KO}} > 0$ suggesting stabilization by the thermal trapped ions alone. This would be consistent with the observed lack of unchange in the ST behavior when the FW is applied. But, it is inconsistent with the observation of actual sawtoothing behavior in this discharge. Consistency would require $\delta\hat{W}_{\mathrm{MHD}} + \delta\hat{W}_{\mathrm{KO}} < 0$ and $\delta\hat{W}_{\mathrm{MHD}} + \delta\hat{W}_{\mathrm{KO}} + \delta\hat{W}_{\mathrm{fast}} < 0$.

There are a number of other reasons any one of which would account for the remaining disagreement. First, the results can be sensitive to the estimates for the equilibrium parameters – s_1, κ_1, ε_1, and q_0 which appear directly in the criteria – but also the equilibrium profiles which appear implicitly through the profiles in the $\delta\hat{W}$ contributions. Near marginal stability, small changes in these quantities can produce order of magnitude variations in $\delta\hat{W}_{\mathrm{MHD}}$. Second, assumptions built into the models can be violated. In particular, the Bussac calculation and its extensions assume that $r_1/a \sim 1$ and $q_0 - 1 \sim \varepsilon$, with a resulting "top hat" eigenfunction, in which case $\gamma_{\mathrm{MHD}}\tau_{\mathrm{A}} \sim \delta\hat{W}_{\mathrm{MHD}}$. The numerical calculations generally do not reproduce this scaling except in the limiting large aspect ratio case near marginal stability [13-16].

The numerically computed growth rates from $(\delta W/\delta K)^{1/2}$, and the $\delta\hat{W}$ values calculated from δW, plus the estimated values of s_1, ε_1, and $|\xi_0|^2$, yield considerably more unstable predictions than either of the estimates for $\delta\hat{W}_{\mathrm{MHD}}$ in Table 2. These would predict instability with no possibility of stabilization by any non-ideal effect. In the case of #122080, this can be attributed to the eigenmode not reproducing the "top-hat" structure. Figure 4 shows the mode displacements from the GATO code for the two reconstructed equilibria. For #96043, there is some deviation but the top hat appears to be a reasonable approximation. Sensitivity calculations with independently varying q_0 and r_1 show that the important quantity in determining the top hat structure is r_1. Nevertheless, for both discharges, $\gamma\tau_{\mathrm{A}}$ calculated from $(\delta W/\delta K)^{1/2}$ is quite different from $\delta\hat{W}_{\mathrm{MHD}}$ using any reasonable estimates for r_1 and s_1. This is an

indication that the assumption that all the inertia is in the thin layer around $q = 1$ and can be estimated using the cylindrical approximation to $\nabla \cdot \xi = 0$, is not valid.

The presence of a vacuum region is known to increase $\delta\hat{W}_{\mathrm{MHD}}$ and $\gamma_{\mathrm{MHD}}\tau_{\mathrm{A}}$ substantially [13-15]. In the discharges considered here, moving the wall to the position of the DIII-D vacuum vessel increases the values of $\delta\hat{W}$ by a factor of roughly two, but nearer marginal stability, this can be an order of magnitude or more. Finally, other non-ideal effects can provide stabilization. Primary among these is sheared plasma rotation, which is significant in DIII-D but is not accounted for.

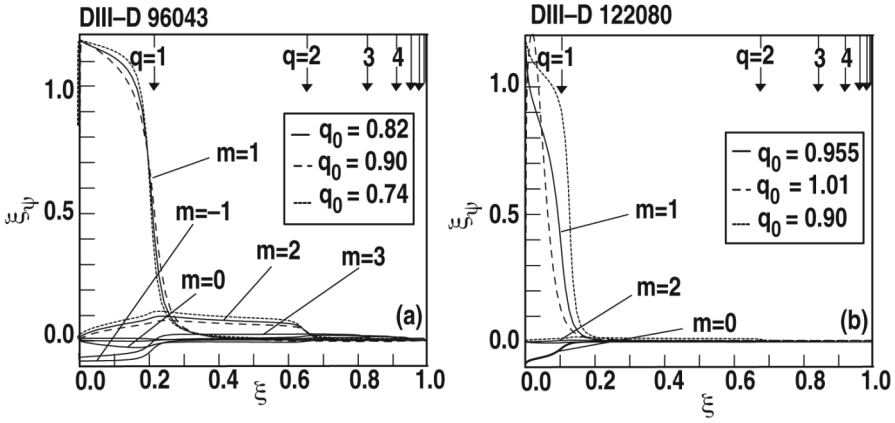

FIGURE 4. Numerically computed internal kink mode structures for the two discharges (a) #96043 and (b) #122080. Shown in both are the results using the best fit to the equilibrium (solid curves) and the two constrained fits with lower (dotted) and higher q_0 (dashed).

6. DISCUSSION

The results described in Section 5 are encouraging but a meaningful comparison of the calculations with the DIII-D experiments, enabling a discrimination between the predictions of the calculated distribution functions, requires more work. The model for δW_{MHD} is the most crucial element at present. The improvement in the consistency obtained for both discharges by using the fitted approximation from Ref. [15] is suggestive that the goal is attainable. The key remaining discrepancy appears to be due to the non "top hat" eigenmode for discharge #122080, which is not incorporated into the fit. The ultimate solution is to utilize the numerically computed $\delta\hat{W}$ for the equilibrium fit in both cases. This should be done as well in estimating $\delta\hat{W}_{\mathrm{KO}}$ and $\delta\hat{W}_{\mathrm{fast}}$ by convolving the distribution functions with the computed eigenmodes.

The key issue in such an analysis is that the equilibria do not yield growth rates sufficiently small to be in the regime where $\gamma_{\mathrm{MHD}}\tau_{\mathrm{A}} \sim \delta\hat{W}_{\mathrm{MHD}}$. This will require obtaining accurate discharge reconstructions sufficiently close to marginal stability. This may require a full analysis through a sizable fraction of the ST cycle. The numerical tools can then be used to discriminate various physics effects, including the different fast particle distributions, as well as other issues such as the presence of a real vacuum region and non-ideal effects.

ACKNOWLEDGMENTS

This work was supported by the U.S. Department of Energy under grant DE-FG03-95ER54309.

REFERENCES

1. R. I. Pinsker, et al., "Absorption of Fast Waves at Moderate to High Ion Cyclotron Harmonics on DIII-D," Proceedings of the 16th Topical Conf. on Radio Frequency Power in Plasmas, Park City, Utah (2005).
2. A. D. Turnbull, et al., "Predictive Capability of MHD Stability Limits in High Performance DIII-D Discharges," *Nucl. Fusion* **42**, 917 (2002).
3. A. D. Turnbull, et al., "Theory and Simulation Basis for Magnetohydrodynamic Stability in DIII–D," *Fusion Sci. Technol.* **48**, 875 (2005).
4. F. Porcelli, D. Boucher, and M. N. Rosenbluth, "Model for the Sawtooth Period and Amplitude," *Plasma Phys. Control. Fusion* **38**, 2163 (1996).
5. R. B. White, *The Theory of Toroidally Confined Plasmas*, Second Edition, London: Imperial College Press, 2001.
6. K. G. McClekments, R. O. Dendy, C. G. Gimblett, R. J. Hastie, and T. J. Martin, "Stabilization of the Ideal m=1 Internal Kink by Alpha Particles and ICRF Heated Ions," *Nucl. Fusion* **35**, 1761 (1995).
7. M. J. Mantsinen, S. Sharapov, B. Alper, A. Gondhalekar, and D. C. McDonald, "A New Type of MHD Activity in JET ICRF-Only Discharges With High Fast-Ion Energy Contents," *Plasma Phys. Control. Fusion* **42**, 1291 (2000).
8. L.-G. Eriksson, et al., " Destabilization of Fast-Ion-Induced Long Sawteeth by Localized Current Drive in the JET Tokamak," *Phys. Rev. Lett.* **92**, 235004 (2004).
9. F. Porcelli, et al., "Modeling of Macroscopic Magnetic Islands in Tokamaks," *Nucl. Fusion* **41**, 1207 (2001).
10. M. N. Bussac, R. Pellat, D. Edery, and J. L. Soulé. *Phys. Rev. Lett.* **35**, 1638 (1975).
11. J. P. Graves, "Influence of Asymmetric Energetic Ion Distributions on Sawtooth Stabilization," *Phys. Rev. Lett.* **92**, 185003 (2004).
12. C. Wahlberg, "Analytical Stability Condition for the Ideal m=n=1 Kink Mode in a Toroidal Plasma With elliptic Cross Section," Phys. Plasmas **5**, 1387 (1998).
13. A. D. Turnbull and F. Troyon, "Toroidal Effects on Current Driven Modes in Tokamaks," *Nucl. Fusion* **29**, 1887 (1989).
14. A. D. Turnbull, "Toroidal Kink Mode at Finite Beta," *Nucl. Fusion* **31**, 2153 (1991).
15. A. Martynov, J. P. Graves, and O. Sauter, "The Stability of the Ideal Internal Kink Mode in Realistic Tokamak Geometry," *Plasma Phys. Control. Fusion* **47**, 1743 (2005).
16. W. Kerner, R. Gruber, and F. Troyon, "Numerical Study of the Internal Kink Mode in Tokamaks," *Phys. Rev. Lett.* **44**, 536 (1980).
17. M. Choi, et al., "Monte-Carlo Orbit/Full Wave Simulation of Fast Alfvén Wave (FW) Damping on Resonant Ions in Tokamaks," Proceedings of the 16th Topical Conf. on Radio Frequency Power in Plasmas, Park City, Utah (2005).
18. M. Brambilla, "`Quasi-local' Wave Equations in Toroidal Geometry With Applications to Fast Wave Propagation and Absorption at High Harmonics of the Ion Cyclotron Frequency," *Plasma Phys. Control. Fusion* **44**, 2423 (2002).
19. C. Angioni, et al., "Neutral Beam stabilization of Sawtooth Oscillations in JET," *Plasma Phys. Control. Fusion* **44**, 205 (2002).
20. J. P. Graves, O. Sauter, N. N. Gorelenkov, "The Internal Kink Mode in an Anisotropic Flowing Plasma With Application to Modeling Neutral Beam Injected Sawtoothing Discharges," *Phys. Plasmas* **10**, 1034 (2003).
21. J. P. Graves, "Internal Kink Mode Stabilization and the Properties of Auxiliary Heated Ions," *Phys. Plasmas* **12**, 090908 (2005).
22. H. Reimerdes, et al., "Effect of Triangular and Elongated Plasma Shape on the Sawtooth Stability," *Plasma Phys. Control. Fusion* **42**, 629 (2000).
23. M. N. Rosenbluth, R. Y. Dagazian, and P. H. Rutherford, "Nonlinear Properties of the Internal m=1 Kink Instability in the Cylindrical Tokamak," *Phys. Fluids* **16**, 1894 (1973).
24. L. C. Bernard, F. J. Helton, and R. W. Moore, "GATO: An MHD Stability Code for Axisymmetric Plasmas With Internal Separatrices," *Comput. Phys. Commun.* **21**, 377 (1981).